Operation and Selection of Multilevel Power Converters for Doubly Fed Induction Generator-based Wind Turbines

Kapil Jha[1], Joseph Banda[2], Hridya I[1], Arvind Tiwari[3]
[1]GE Research, Bangalore, KA, India
[2]Norwegian University Of Science And Technology, Norway
[3]GE Research, Niskayuna, NY, USA
E-Mail: kapil.jha@ge.com

Keywords

DFIG, Wind Energy, Multi-level Converter, ANPC Converter, NPC Converter

Abstract

Operation of Doubly fed induction generator (DFIG) based wind turbine with 3-Level back-to-back converter has been discussed. Converter operation and loss analysis on a 3.2 MW-60Hz turbine shows that classical NPC converter is suitable for line side converter, while Active-NPC (ANPC) converter is optimal for rotor side converter realization.

Introduction

Conventionally, 2-level voltage source converters are used in building back-back power electronic system for DFIG based turbines [1] due to their cost, reliability, and performance. To reduce overall levelized cost of electricity, wind turbine manufacturers are continuously targeting for higher output power from individual turbine. As the turbine power increase, the voltage and/or current rating of the back-back converter system need to increase as well. Higher current in electrical system leads to higher losses, hence, at certain power level it becomes imperative to use converters which can produce higher voltage reliably. In this paper, operation of multi-level converter with DFIG has been evaluated.

Several multilevel converter topologies have been proposed in literature to generate higher output voltage, e.g. NPC and Active-NPC converter, flying capacitor based multilevel converter, neutral point piloted converter, cascaded H-bridge multilevel inverter, etc. [2]. Neutral point clamped (NPC) and Active-NPC (ANPC) converters, are widely used in industry due their performance and reliability. In this paper, operation of NPC and ANPC converters with DFIG based wind turbine have been critically evaluated and converter selection has been suggested accordingly.

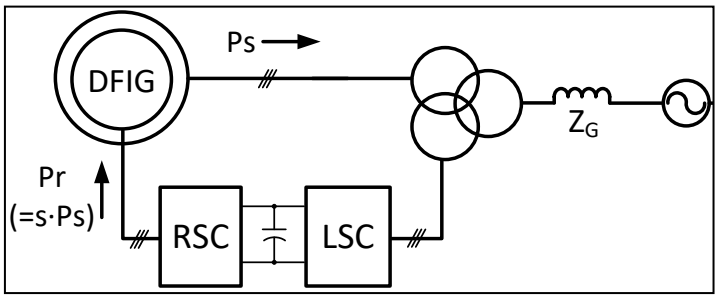

Fig. 1: Electrical single line schematic of DFIG based wind turbine

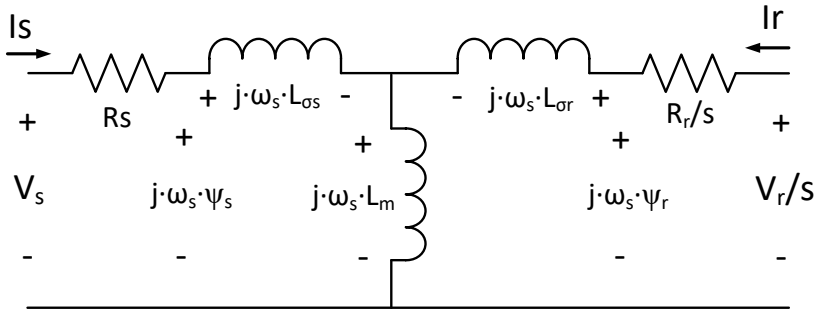

Fig. 2: One phase Steady-state equivalent circuit of doubly fed induction generator referred to stator

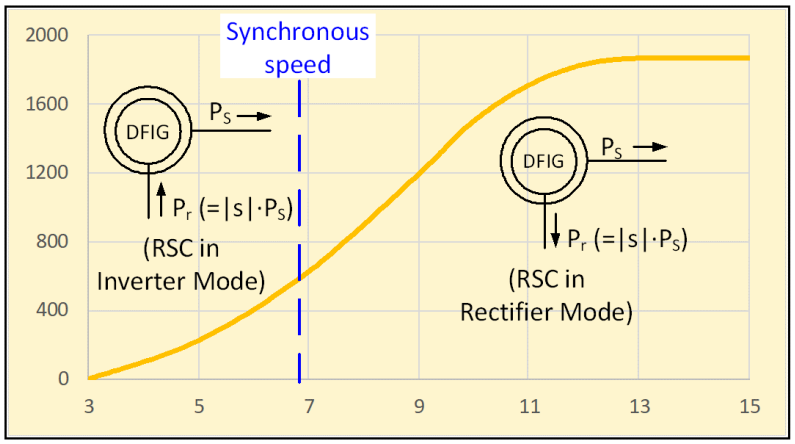

Fig. 3: Sub-synchronous and super-synchronous operation and direction of power flow in DFIG

Overview of DFIG based wind turbine system and operating regions

A simple single line electrical architecture of a doubly fed induction generator (DFIG) based wind turbine with key components is shown in Fig 1. Here, DFIG stator is connected directly to the grid while rotor is coupled to a back-back bidirectional power electronic converter system, viz., the rotor side converter and line side converter. Purpose of the rotor side converter is to generate appropriate rotor voltage at its terminals to generate desired real and reactive power from DFIG. The line side converter controls the shared dc-link of back-back converter system.

One phase equivalent circuit of DFIG in stator reference frame is shown in Fig. 2 [3]. Here, V_S and V_r are stator and rotor voltages, I_s and I_r are stator and rotor currents, respectively. R_s and R_r are stator and rotor resistances, $L_{\sigma s}$ and $L_{\sigma r}$ are stator and rotor leakage inductances,

Table 1: Steady-state expressions of DFIG voltages, currents, and fluxes in stator reference frame

$\bar{V}_s - \bar{I}_s \cdot R_s = j \cdot \omega_s \cdot \bar{\Psi}_s$ (1)	$\bar{V}_r - \bar{I}_r \cdot R_s = j \cdot s \cdot \omega_s \cdot \bar{\Psi}_r$ (4)	$P_r = s \cdot P_s$ (7)
$\bar{\Psi}_s = \bar{I}_s \cdot L_s + \bar{I}_R \cdot L_m$ (2)	$L_s = L_{\sigma s} + L_m$ (5)	$P_{mech} = P_s + P_r$ (8)
$\bar{\Psi}_R = \bar{I}_s \cdot L_m + \bar{I}_R \cdot L_r$ (3)	$L_r = L_{\sigma r} + L_m$ (6)	

Table 2: DFIG voltage, current and flux phasors in under-excited, UPF, and over-excited conditions at sub-synchronous and super-synchronous operations

	under-excited (Qs < 0)	UPF (Qs = 0)	over-excited (Qs > 0)
Sub-Synchronous Operation (s > 0)	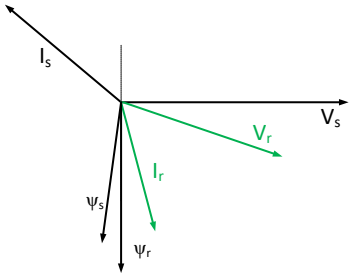	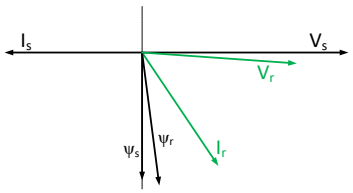	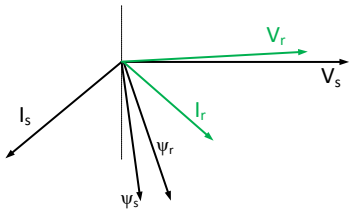
Super-Synchronous Operation (s < 0)	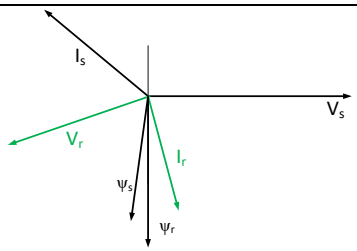	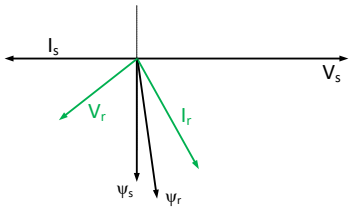	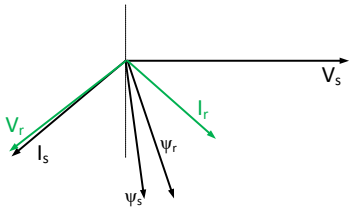

L_s and L_r are stator and rotor inductances, respectively. ω_s is grid voltage angular speed, *s* is slip of operation, and L_m is the magnetizing inductance. Ψ_s and Ψ_r are stator and rotor fluxes, respectively.

Steady state expressions of voltages and fluxes are given in (1) – (8) for DFIG machine in stator referred reference frame in Table 1. Using these equations, steady-state magnitudes of fluxes, power, and currents of the machine can be determined at any given machine parameters, speed, and voltages.

It is an inherent property of DFIG that partial power of stator flows through the rotor (7), as shown in Fig. 3 [4]. The magnetizing current for the DFIG is provided by RSC. In sub-synchronous operation, the RSC operates in inverter mode while in super-synchronous operation it acts as a rectifier at various power factors. Region specific grid code requires a wind turbine to support rated reactive power across all operating points [5]. The phasor plots at under-excited, unity power factor (UPF), and over-excited condition for DFIG at sub-synchronous as well as super-synchronous speed have been plotted in Table 2. Here, Qs is the reactive power output from DFIG stator. In sub-synchronous operation, both V_r and I_r are in positive half of phasor plot suggesting inverter mode operation for RSC. While, in super-synchronous operation, V_r and I_r are in opposite half of each other indicating rectifier mode of operation for RSC. Hence, RSC operates both at leading as well as lagging power factor. In contrast, LSC usually operates at fixed power factor, depending upon speed of the DFIG. In sub-synchronous operation LSC operates in rectifier mode at -1 power factor, while, it operates in inverter mode at UPF at super-synchronous speed.

Selection of NPC vs ANPC converter for DFIG

In schematic of Fig. 4(a), one phase leg of neutral point clamped converter is shown. Here, T1-T6 are power semiconductor devices. In NPC converter, T1-T4 are active switches (IGBT/IGCT/Power MOSFET), with antiparallel diode, while T5 and T6 are power diodes. In an ANPC converter, all six switches (T1-T6) are active switches with antiparallel diodes, and this configuration provide additional option to distribute the losses using controls [6-7].

Table 3: System parameters for simulation validation

Attribute	Value
P_{mech} (MW)	3.2
Qs (MVar)	1.0
f (Hz)	60
Poles	6
ω (RPM)	1500
s	-0.25
IGBT module with diode	FZ3600R17HP4
Dc-link (V)	~2200
f_{sw}	2 kHz

1. Modulation and Switching

The switching scheme of active power semiconductor switches is mentioned in Table 3 (a) and (b) for NPC and ANPC converters. The sine-triangle modulation scheme has been used to generate the switching pattern, where the modulation signal of low frequency is compared with higher frequency triangular carrier signal to generate switching output. Here *m* is the modulation index and *S* is the switching state. *S* is logic high at an instant when *m* is higher than the carrier triangular signal and vice versa. $\bar{S}$ is complementary signal of *S,* as shown in Fig. 4(b).

2. Commutation path

The commutation path for NPC as well as ANPC converters have been evaluated to analyze the operation under non-UPF condition. It is important to note that both in NPC as well as ANPC converter, the voltages and current through the device T1 and T4 will remain same at similar operating condition. Only difference in current and power distribution will occur in devices T2, T3, T5, and T6. The commutation path has been plotted at an instant of $m>0$ in rectifier mode, as shown in Fig. 5. In Fig. 5(a), when S is logic high, the current flows into the capacitors via diodes of T1 and T2 and when S is logic low, current flows into the neutral mid-point via T3 and T6. However, in ANPC converter both in positive and zero state, the current flows through it as shown in Fig. 5(b). Hence, in NPC converter, significant switching losses occur in T2 along with conduction losses, however, in ANPC converter, no switching loss would occur in device T2. The conduction losses will be identical in NPC and ANPC converters in rectifier mode operation. However, in rectifier operation, switching losses will be lower in ANPC converter as compared to NPC converter. In ANPC converter, switching losses will occur in devices T1 and T5 in positive half of modulation ($m>0$), however, in NPC converter switching losses will occur in devices T1, T2, T3, and T6. Hence, total losses in ANPC converter will also be lower as compared to NPC in rectifier mode of operation.

Table 4: Switching pattern for (a) NPC and (b) ANPC converter

(a)

NPC	s1	s2	s3	s4
$m\geq 0$	*S*	1	$\bar{S}$	0
$m<0$	0	$\bar{S}$	1	*S*

(b)

ANPC	s1	s2	s3	s4	s5	s6
$m\geq 0$	*S*	1	0	0	$\bar{S}$	*S*
$m<0$	0	0	1	*S*	*S*	$\bar{S}$

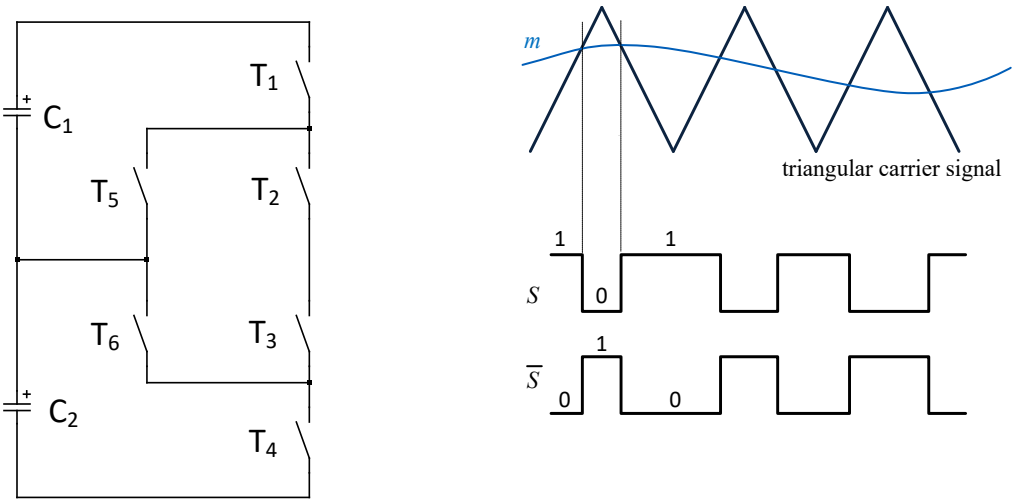

(a) (b)

Fig. 4: (a) Generic schematic of neutral point clamped converters; (b) Synthesis of switching pulses

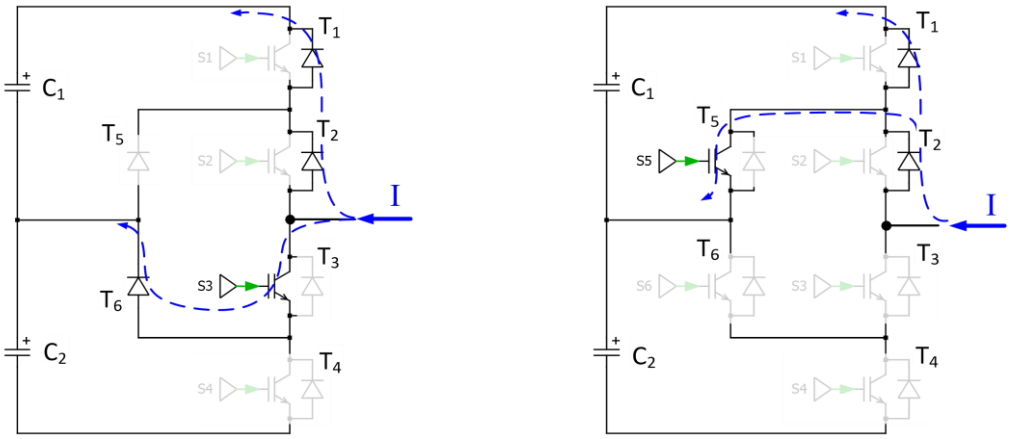

(a) (b)

Fig. 5: Current flow direction in (a) NPC and (b) ANPC converter in rectifier mode of operation during active and zero states

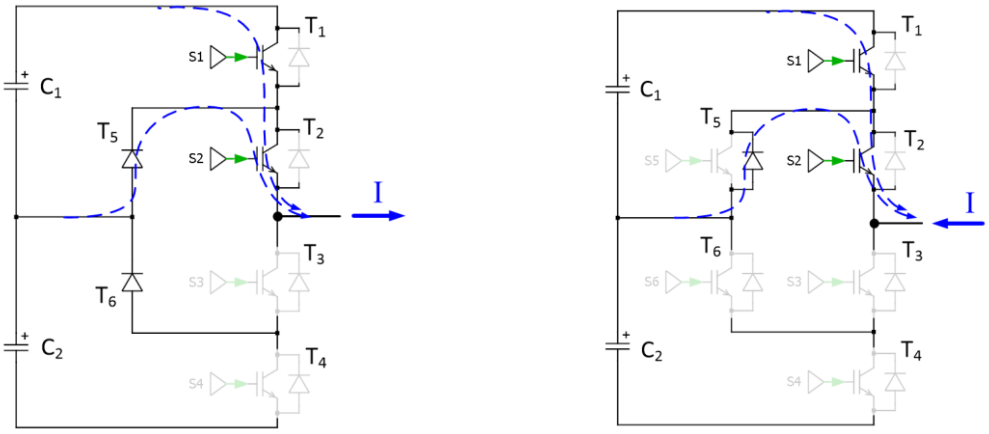

(a) (b)

Fig. 6: Current flow direction in (a) NPC and (b) ANPC converter in inverter mode of operation during active and zero states

3. Loss Analysis and Converter Selection

The RSC process maximum power at rated operation of turbine in super-synchronous region and both RSC and LSC converter ratings and thermal requirements are designed for the same. Since both NPC and ANPC converters are identical except for switches T5 and T6, losses in switches T1 and T4 will remain the same for both converters at same operating conditions. However, the loss distribution will be different in switches T2, T3, T5, and T6.

Specifications of the rated operation are mentioned in Table 4. Here, P_{mech} is DFIG output power in megawatts, it is combination of P_s and P_r as given by (8). Qs is the DFIG stator reactive power output in MVar. Grid frequency (f) is 60 Hz, and DFIG synchronous speed is 1200 RPM. At rated operation, machine is rotated at 1500 RPM at -0.25 slip. The dc-link is maintained at 2.2 kV for both NPC as well as ANPC converters. RSC switching frequency is 2 kHz.

Comparison of loss distribution in NPC and ANPC converters has been done for RSC, as shown in Fig. 7. Here, phase modulation (m), output current (I_r), conduction losses (P_{cond}), switching losses (P_{sw}), and total losses (P_{Tot}) have been plotted in devices T2 and T5 for both NPC and ANPC converters, as shown in Fig. 7(a) and Fig. 7(b), respectively. It is important to recall that in device T2 in NPC and ANPC converters represents IGBT+anti-parallel diode, however, device T5 in NPC is diode while device T5 in ANPC converter is IGBT+anti-parallel diode, as shown in Fig. 5. Losses in Fig. 7 are combination of both IGBT and diode, wherever applicable.

As shown in Fig. 7, combined total losses in NPC converter of devices T2 and T5 (P_{Tot_T2} + P_{Tot_T5}) are more than 20% higher as compared to combined losses of devices T2 and T5 in ANPC converter, due to higher switching losses in NPC converter. As discussed previously, device T2 in RSC realized using NPC converter will experience both conduction and switching losses, at rated operation, as shown in Fig. 7(a). Here, device T2 bears approx. 75% of combined total losses of devices T2 and T5. The cooling requirements for this converter needs to be designed as per total losses in device T2.

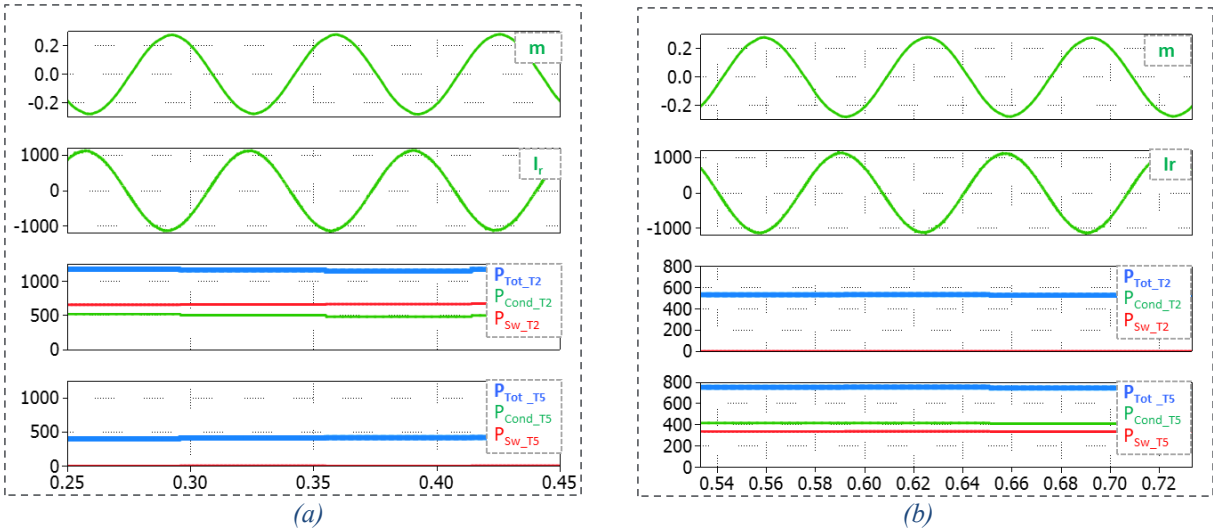

(a) *(b)*

Fig. 7: At Rated Power condition, total transistor losses at T2 and T5 - in (a) NPC and (b) ANPC based 3-level converter

Table 5: Comparison of ANPC vs NPC converter for RSC realization

Total Losses	ANPC converter has 20% lower losses as compared to NPC converter
Max device losses	35% less in ANPC converter as compared to NPC converter
Loss distribution (T2:T5)	75:25 in NPC vs 41:59 in ANPC

However, in case of ANPC converter, as shown in Fig. 7(b), using the switching pattern described in Table 3(b), T2 device only observe conduction losses. Here, device T2 bears approx. 41% of combined total losses of devices T2 and T5. In this way, both T2 and T5 devices in ANPC converter are significantly less-stressed as compared to NPC converter. Therefore, ANPC converter cooling requirement would be much lesser as compared to NPC converter, also, efficiency of ANPC converter would also be better. Maximum thermal losses in a device in ANPC converter are approximately 35% lower than maximum thermal losses in NPC converter, which significantly reduces cooling requirements in ANPC converter. same has been summarized in Table 5. Hence, ANPC converter is better suited for RSC realization.

LSC in DFIG operates in inverter mode at rated condition which usually operates at UPF. Both NPC and ANPC converters will observe same loss distribution in LSC and same total losses as well, as shown in Fig. 6. Hence, NPC is more suitable to realize LSC as it requires lower active switches and cost saving is possible as NPC requires lower number of control and gate drive cards as compared to ANPC converter.

Conclusion

In this paper, operation of DFIG and variant of neutral point clamped multi-level converters have been discussed. Based upon the thermal and loss analysis, classic neutral point clamped converter appears more suitable for realization of line side converter in DFIG turbine while active-NPC converter is optimal for realization of rotor side converter. Simulation validation of the results with a 3.2 MW-60Hz DFIG turbine at rated operation show that maximum losses in individual device can be reduced by 35% in RSC with ANPC converter as compared to NPC converter, and efficiency of system also increases. NPC converter has been chosen for LSC as both loss distribution and efficiency in ANPC and NPC converter are found to be identical at rated power operation of DFIG.

References

[1] J. M. Carrasco, L. G. Franquelo, J. T. Bialasiewicz, E. Galvan, R. C. Portillo Guisado, M. A. M. Prats, J. I. Leon, N. Moreno-Alfonso, "Power-electronic systems for the grid integration of renewable energy sources: a survey", IEEE Trans. on Ind. Electron., vol. 53, no. 4, pp. 1002-1016, June 2006.

[2] S. S. Fazel, S. Bernet, D. Krug, and K. Jalili, “Design and Comparison of 4-kV Neutral-Point-Clamped, Flying-Capacitor, and Series-Connected H-Bridge Multilevel Converters,” IEEE Trans. on Ind. Electronics, vol. 43, no. 4, pp. 1032-1040, July 2007.

[3] G. Abad, J. López, M. Rodríguez, L. Marroyo, G. Iwanski, Doubly Fed Induction Machine: Modeling and Control for Wind Energy Generation Applications, Wiley-IEEE Press, 2011.

[4] “GE’s 1.87-87,” GE Renewable Energy. [Online]. Available: https://www.ge.com/content/dam/ge-renew-new/downloads/brochures/wind-onshore-turbine-1.85-87-gea30627d-r1.pdf

[5] E. H. Enrique, “Generation Capability Curves for Wind Farms,” IEEE Conf. on Technologies for Sustainability (SusTech), pp. 103-106, July 2014.

[6] T. Brückner, S. Bernet, and H. Güldner, “The Active NPC Converter and Its Loss-Balancing Control,” IEEE Trans. on Ind. Electronics, vol. 52, no. 3, pp. 855-868, June 2005.

[7] Y. Deng, J. Li, K. H. Shin, et. al, “Improved modulation scheme for loss balancing of three-level active NPC converters,” IEEE Trans. Power Electron., vol. 32, no. 4, pp. 2521–2532, Apr. 2017.